Available online at www.sciencedirect.com
SCIENCE DIRECT®
ELSEVIER
International Journal of Multiphase Flow 30 (2004) 181–198
International Journal of Multiphase Flow
www.elsevier.com/locate/ijmulflow

Numerical research on a vaporizing fuel droplet in a forced convective environment

Hongtao Zhang *

Department of Mechanical Engineering, University of Nebraska-Lincoln, Lincoln, NE 68588-0656, USA

Received 10 July 2003; received in revised form 15 November 2003

Abstract

A comprehensive numerical model is developed to study a vaporizing *n*-heptane droplet in a forced convective environment under different temperature conditions, which includes high-pressure effects, liquid phase internal circulation, variable thermophysical properties, solubility of inert species into the liquid phase, and gas and liquid phase transients. Numerical predications of time histories of the dimensionless diameter square of a vaporizing fuel droplet within a zero gravity environment are in very good agreement with the micro-gravity experimental data.

The numerical results show that at higher ambient pressure (such as 4 MPa) the droplet swells initially due to the heat-up of the cold droplet and its subsequent regression rate is far from following the d^2-law during the early stages of droplet evaporation. However, at the ambient pressure of 0.1 MPa, the droplet swells are not obvious. The droplet presents an almost d^2-law behavior in later stages of droplet evaporation for all considered pressures (up to 4 MPa). The numerical results also show that the droplet lifetime decreases with increasing ambient temperature. For example, the droplet lifetime at the ambient temperature 1200 K can be only 50–60% of the droplet lifetime at the ambient temperature 600 K. The final penetration distance of the vaporizing droplet decreases almost linearly with the ambient temperatures considered.

Keywords: Evaporation; Fuel droplet; Forced convection

1. Introduction

Energy is the key research subject in the world and energy is the base of all civilization. The most part of the world's energy is supplied by the combustion of fuels such as gasoline, heavy oils,

* Tel.: +1-402-472-6393; fax: +1-402-472-1465.
E-mail address: hzhang3@unl.edu (H. Zhang).

0301-9322/$ - see front matter
doi:10.1016/j.ijmultiphaseflow.2003.11.005

coal and natural gas. Fuel evaporation is very important in fuel combustion process. For examples, in order for a fuel such as gasoline to burn, it must be evaporated. Liquid gasoline does not burn, only the vapors of fuel do. Fuel evaporation is part of a larger problem—achieving a better physical understanding and a more accurate treatment of the phenomenon of spray combustion. When a liquid fuel droplet is injected into a combustion chamber, it will first evaporate within the chamber gas. Practical interest in the evaporation and combustion of liquid fuel sprays has led to the need for a detailed understanding of the evaporation of a moving droplet at intermediate Reynolds numbers ($Re = O(100)$). Re is defined by $\rho dV/\mu$, here, ρ is density, d is droplet diameter, V is gas velocity, and μ is gas viscosity. During recent years, important progress has been made in the understanding of single droplet behavior and gas–liquid interaction within a spray combustion system. Sophisticated computational fluid dynamics (CFD) models have been used to derive the interface exchange coefficients between a liquid propellant droplet and the surrounding hot combustion gas, such as drag coefficient, mass transfer rate, and energy transfer rate. These research results are very important in further understanding of fuel combustion, optimizing design of engines that propel missiles, jets, and many other industrial devices, and thus improving the fuel combustion efficiency and productive use of natural resources.

A good way to study droplet's dynamics is to study the dynamics of a single droplet that provides details of the fine scales of the relevant phenomena, such as drag coefficient, heat transfer rate, evaporation constant, penetration distance and droplet lifetime. During the past decades, important progress (Faeth, 1977; Law, 1982; Faeth, 1983; Sirignano, 1983; Dwyer, 1989; Givler and Abraham, 1996) has been made in understanding single droplet behavior. Under the assumption that droplets maintain spherical shapes, there are many studies available on moving droplets evaporating within a low-pressure environment. For example, Prakash and Sirignano (1980) used boundary layer analysis with unsteady heat transfer in the circulating liquid phase to examine evaporation of *n*-hexane, *n*-decane, and *n*-hexadecane droplets. Renksizbulut and Yuen (1983) conducted a variable-property analysis of droplet evaporation assuming quasi-steady gas-phase behavior and negligible liquid phase motion and heating. Haywood et al. (1989), Megaridis and Sirignano (1990), and Chiang et al. (1992) extensively examine the gas and liquid phase transient processes in convective droplet evaporation.

Some experimental studies have addressed the pressure effects on the droplet evaporation constant of droplet evaporation/burning. Sato et al. (1990) experimentally studied burning of a suspended droplet under either normal gravity or micro-gravity. The experiments of Nomura et al. (1996) measured (d/d_0^2) of *n*-heptane droplets with time for different ambient pressures and temperatures under micro-gravity conditions. Numerical research on droplet evaporation at high pressures has been mostly limited to stagnant surroundings. Matlosz et al. (1972), Rosner and Chang (1973), Kadota and Hiroyasu (1976), Delplanque and Sirignano (1991), and Arias-Zugast et al. (2000) assumed that the ambient gas does not dissolve into the liquid droplet. Manrique and Borman (1969), Canada and Faeth (1973), Curtis and Farrell (1992), Delplanque and Sirignano (1993), Hsieh et al. (1991), Poplow (1994), and Haldenwang et al. (1996) examine various aspects of high pressure droplet evaporation under stagnant ambient conditions while allowing for inert species solubility in the liquid phase. Supercritical droplet evaporation and combustion studies have been recently reviewed by Givler and Abraham (1996). However, these researchers developed their model of droplet evaporation using one-dimensional, spherically symmetric assumption in the stagnant environment, not in the convective environment.

The actual spray evaporation of droplet takes place in convective sub- or super-critical conditions. Therefore, not only the high-pressure effects, but also the convective effects are to be considered in the numerical model. The droplet evaporation under convective environment is a complex process. At the early period, Convective and diffusive effects are major effects, which control the evaporation process. However, conduction effects cannot be neglected at the later period of the droplet evaporation and high-pressure conditions. These opinions and results may be found in the review papers by Law (1982); Faeth (1983), Givler and Abraham (1996). Therefore, many efforts have made to include all these effects in the current model. Recently, Zhang (2000) studied the moving droplet evaporation in high-pressure and high-temperature environments. This model includes high-pressure effects, real gas effects, liquid phase internal circulation, variable thermophysical properties, solubility of inert species into the liquid phase, and gas and liquid phase transients by employing the criterion that the droplet remains nearly spherical for Weber numbers less than 1.0 even when the Reynolds number is up to 400, which was reported by Dandy and Leal (1989). Here, Weber number represents the ratio of external aerodynamic force to the surface tension force. By definition, $We = \rho V d/\sigma$, where ρ is the gas density, d is the diameter of the droplet, V is the gas velocity relative to the droplet, and σ is the surface tension.

Based on the model developed by Zhang (2000), preliminary results are discussed by Zhang and Gogos (2001). This paper further presents the effects of different temperature conditions on the evaporation of the liquid *n*-heptane droplet under forced convection, such as effects on droplet lifetime, droplet evaporation constant, and droplet penetration distance.

2. Theoretical model

A liquid fuel droplet of initial radius R_0 is evaporating in a forced convection environment of infinite expanse. The initial temperature of the droplet is T_0, and the ambient pressure and temperature are p_∞ and T_∞, respectively. Consequently, the convective motion present in the gas phase is that induced by flowing gas in the forced convection environment and evaporation of fuel droplet. A typical vaporizing droplet under a forced convective environment is plotted in Fig. 1. The streamlines of gas and liquid phases are plotted in Fig. 1. The liquid droplet is *n*-heptane with initial temperature 300 K and initial diameter 0.1 mm. The surrounding gas is nitrogen with inflow temperature 1000 K under atmospheric pressure of 3 MPa. In the following analysis, binary system (*n*-heptane and N_2), internal circulation, variable properties, transient effects, high temperature and high-pressure effects are all considered. The changes in the liquid phase density are due to both thermal expansion and change in species. In the analysis, we assume: (1) the droplet shape always remains spherical, (2) radiation energy is negligible, (3) second-order effects, such as the Soret and Dufour effects are neglected, (4) viscous dissipation is neglected, and (5) the flow field is laminar and axisymmetric.

In the current model, there are axisymmetric unsteady equations of mass, species, momentum, and energy conservation in the both gas and liquid phases. These detailed governing equations are list in the reference by Zhang (2000). The following dimensionless quantities are used in the spherical coordinate (*note:* * stands for dimensional parameter in the following sections):

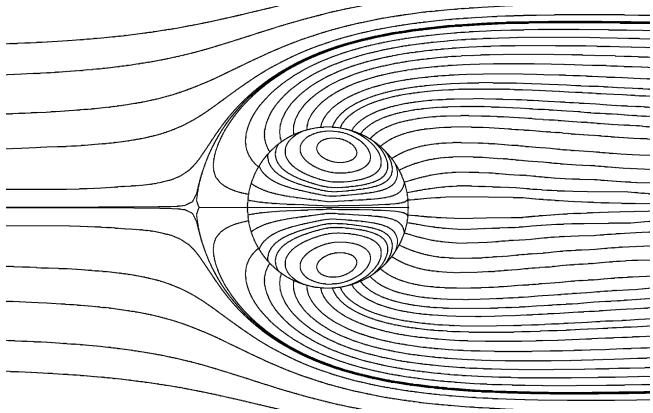

Fig. 1. A typical vaporizing droplet under a forced convective environment.

$$\rho = \frac{\rho^*}{\rho^*_\infty}, \quad \mu = \frac{\mu^*}{\mu^*_\infty}, \quad k = \frac{k^*}{k^*_\infty}, \quad D_{12} = \frac{D^*_{12}}{D^*_{12,\infty}}$$

$$c_\mathrm{p} = \frac{c^*_\mathrm{p}}{c^*_{\mathrm{p},\infty}}, \quad V = \frac{V^*_\infty}{V^*_{\infty,0}}, \quad V_r = \frac{V^*_r}{V^*_\infty}, \quad V_\theta = \frac{V^*_\theta}{V^*_\infty}$$

$$t = \frac{t^*}{R^{*2}_0/v^*_\infty}, \quad h_i = \frac{h^*_i}{c^*_{\mathrm{p},\infty}(T^*_\infty - T^*_0)}, \quad p = \frac{p^* - p^*_\infty}{\rho^*_\infty V^{*2}_{\infty,0}}$$

$$T = \frac{T^*_\infty - T^*}{T^*_\infty - T^*_0}, \quad R = \frac{R^*}{R^*_0}, \quad r = \frac{r^*}{R^*}, \quad \dot{R} = \frac{\dot{R}^*}{v^*_\infty/R^*_0}$$

$$Re_0 = \frac{2\rho^*_\infty R^*_0 V^*_{\infty,0}}{\mu^*_\infty}, \quad Pr = \frac{\rho^*_\infty v^*_\infty c^*_{\mathrm{p},\infty}}{k^*_\infty}, \quad Sc = \frac{v^*_\infty}{D^*_{12,\infty}}$$

$$z = \ln r = \ln \frac{r^*}{R^*}, \quad \dot{m}''_\theta = \frac{\dot{m}''^*_\theta}{\rho^*_\infty V^*_{\infty,0}}, \quad \tau_{rr} = \frac{\mu^*_\infty V^*_{\infty,0}}{R^*_0}\frac{\tau^*_{rr}}{R^*}$$

$$\tau_{\theta\theta} = \frac{\mu^*_\infty V^*_{\infty,0}}{R^*_0}\frac{\tau^*_{\theta\theta}}{R^*}, \quad \tau_{r\theta} = \frac{\mu^*_\infty V^*_{\infty,0}}{R^*_0}\frac{\tau^*_{r\theta}}{R^*}, \quad \tau_{\phi\phi} = \frac{\mu^*_\infty V^*_{\infty,0}}{R^*_0}\frac{\tau^*_{\phi\phi}}{R^*}$$

where ∞ stands for ambient condition, ρ is density, μ is viscosity, k is thermal conductivity, D_{12} is binary diffusion coefficient for species 1 (n-heptane) and 2 (nitrogen), c_p is specific heat at constant pressure, V is velocity, V_r is radial velocity, V_θ is polar velocity, t is time, h_i is specific enthalpy of ith species, p is pressure, T is temperature, r is radial coordinate, R is instantaneous radius of the droplet. $\dot{R}$ is the regression rate of the droplet surface, Re_0 is the initial Reynolds number, Pr is Prandtl number, Sc is Schmidt number, $\dot{m}''_\theta$ is local mass flux of evaporation at the interface, τ_{rr}, $\tau_{\theta\theta}$, $\tau_{r\theta}$, and $\tau_{\phi\phi}$ are stresses in the directions of rr, $\theta\theta$, $r\theta$ and $\phi\phi$, respectively.

After the above dimensionless quantities are applied, the governing equations may take the following single dimensionless form in spherical coordinate:

$$\frac{\partial}{\partial t}(2\rho e^{3z} R\sin\theta V\Phi)+\frac{\partial}{\partial z}\left[\rho e^{2z}\sin\theta V^2\left(Re_0 V_r-2\frac{e^z\dot{R}}{V}\right)\Phi+\frac{\partial}{\partial\theta}\left(\rho e^{2z}\sin\theta Re_0 V^2 V_\theta\Phi\right)\right.$$
$$\left.=\frac{\partial}{\partial z}\left(\Gamma_z\frac{e^z V}{R}\sin\theta\frac{\partial\Phi}{\partial z}\right)+\frac{\partial}{\partial\theta}\left(\Gamma_\theta\frac{e^z V}{R}\sin\theta\frac{\partial\Phi}{\partial\theta}\right)+\delta_{\text{source}}\right].$$

Φ, Γ_z, Γ_θ, and δ_{source} have different values depending on the different governing equations:

(A) continuity equation

$$\Phi=1;\quad \Gamma_z=\Gamma_\theta=0;\quad \delta_{\text{source}}=-4\dot{R}\rho e^{3z}\sin\theta V+2R\rho e^{3z}\sin\theta\frac{dV}{dt}.$$

(B) r-momentum equation

$$\Phi=V_r,\quad \Gamma_z=8/3\mu,\quad \Gamma_\theta=2\mu,$$
$$\delta_{\text{source}}=-e^{2z}\sin\theta Re_0\frac{\partial p}{\partial z}+\rho e^{2z}\sin\theta Re_0 V^2 V_\vartheta^2-4\dot{R}\rho e^{3z}\sin\theta VV_r$$
$$-\frac{\partial}{\partial z}\left[\frac{4\mu}{3}\frac{e^z V\sin\theta}{R}\left(\frac{\partial V_\theta}{\partial\theta}+V_\theta\cot\theta+2V_r\right)\right]+\frac{\partial}{\partial\theta}\left[2\mu\frac{e^z V\sin\theta}{R}\left(\frac{\partial V_\theta}{\partial z}-V_\theta\right)\right]$$
$$-\frac{2e^{2z}\sin\theta}{R}(\tau_{\theta\theta}+\tau_{\phi\phi}).$$

(C) θ-momentum equation

$$\Phi=V_\theta,\quad \Gamma_z=2\mu,\quad \Gamma_\theta=8/3\mu,$$
$$\delta_{\text{source}}=-e^{2z}\sin\theta Re_0\frac{\partial p}{\partial\theta}-\rho e^{2z}\sin\theta Re_0 V^2 V_\theta V_r-4\dot{R}\rho e^{3z}\sin\theta VV_\theta$$
$$-\frac{\partial}{\partial\theta}\left[\frac{4\mu}{3}\frac{e^z V\sin\theta}{R}\left(\frac{\partial V_r}{\partial z}+V_\theta\cot\theta-V_r\right)\right]+\frac{\partial}{\partial z}\left[2\mu\frac{e^z V\sin\theta}{R}\left(\frac{\partial V_r}{\partial\theta}-V_\theta\right)\right]$$
$$+\frac{2e^{2z}\sin\theta}{R}(\tau_{r\theta}+\tau_{\phi\phi}\cot\theta).$$

(D) species equation

$$\Phi=Y_1;\quad \Gamma_z=\Gamma_\theta=2\rho D_{12}/Sc;\quad \delta_{\text{source}}=-4\dot{R}\rho e^{3z}\sin\theta VY_1+2R\rho e^{3z}\sin\theta Y_1\frac{dV}{dt},$$

where Y_1 is the mass fraction of n-heptane.

(E) energy equation

$$\Phi=T;\quad \Gamma_z=\Gamma_\theta=2k/(c_p Pr);$$
$$\delta_{\text{source}}=\frac{2}{c_p Sc}\frac{\partial Y_1}{\partial z}\frac{e^z V\rho\sin\theta}{R}D_{12}\frac{\partial}{\partial z}(h_2-h_1)+\frac{2}{c_p Sc}\frac{\partial Y_1}{\partial\theta}\frac{e^z V\rho\sin\theta}{R}D_{12}\frac{\partial}{\partial\theta}(h_2-h_1)$$
$$-4\dot{R}\rho e^{3z}\sin\theta VT+2R\rho e^{3z}\sin\theta T\frac{dV}{dt},$$

where 1 stands for species 1 (n-heptane), and 2 stands for species 2 (nitrogen).

The above governing equations are solved subject to the following dimensionless boundary conditions:

(a) along axis of symmetry ($\theta = 0$, $\theta = \pi$):

$$\frac{\partial \Phi}{\partial \theta} = 0,$$

where $\Phi = V_r$, T, Y_1.

$$V_\theta = 0.$$

(b) inflow freestream ($r = r_\infty$, $0 \leqslant \theta \leqslant \pi/2$):

$$T = 0,$$

$$Y_1 = Y_{1,\infty},$$

$$V_{\theta,\infty} = \sin\theta,$$

$$V_{r,\infty} = -\cos\theta,$$

(c) outflow freestream ($r = r_\infty$, $\pi/2 \leqslant \theta \leqslant \pi$):

$$\frac{\partial \Phi}{\partial z} = 0.$$

where $\Phi = V_r$, V_θ, T, Y_1.

(d) gas/liquid interface at $r = R(t)$:

1. continuity of temperature:

$$T_{s,l} = T_{s,g},$$

where s stands for the interface condition, l stands for liquid phase, and g stands for gas phase.

2. conservation of mass:

$$V_{r,l,s} = \frac{1}{V}\left(\frac{\dot{m}''_\theta}{\rho_{l,s}} + \frac{2}{Re_0}\frac{dR}{dt}\right),$$

$$V_{r,g,s} = \frac{1}{V}\left(\frac{\dot{m}''_\theta}{\rho_{g,s}} + \frac{2}{Re_0}\frac{dR}{dt}\right).$$

3. conservation of shear stress and continuity of tangential velocity:

$$\tau_{r\theta,l} = \tau_{r\theta,g},$$

$$V_{\theta,g,s} = V_{\theta,l,s}.$$

4. conservation of energy:

$$\dot{m}''_\theta[Y_{1,g,s}(h_{1,g,s}-h_{1,l,s})+Y_{2,g,s}(h_{2,g,s}-h_{2,l,s})]-\frac{2\rho D_{12}}{Re_0 ScR}\left[\frac{\partial Y_{1,g,s}}{\partial z}(h_{1,g,s}-h_{1,l,s})+\frac{\partial Y_{2,g,s}}{\partial z}(h_{2,g,s}-h_{2,l,s})\right]+\frac{2}{Re_0 PrR}\left(k_{g,s}\frac{\partial T}{\partial Z}-k_{l,s}\frac{\partial T}{\partial r}\right)=0.$$

5. conservation of species:

$$\frac{Re_0}{2}\dot{m}''_\theta(Y_{1,g}-Y_{1,l})-\frac{\rho_{g,s}D_{12,g,s}}{ScR}\frac{\partial Y_{1,g}}{\partial z}+\frac{\rho_{l,s}D_{12,l,s}}{ScR}\frac{\partial Y_{1,l}}{\partial r}=0.$$

(e) the overall conservation of mass for the droplet is expressed as

$$\frac{\mathrm{d}R}{\mathrm{d}t}=-\frac{Re_0}{4\bar{\rho}_l}\int_0^\pi \dot{m}''_\theta \sin\theta\,\mathrm{d}\theta-\frac{R}{3\bar{\rho}_l}\frac{\mathrm{d}\bar{\rho}_l}{\mathrm{d}t},$$

where $\bar{\rho}_l$ is the average density of the liquid droplet.

(f) the overall conservation of momentum is

$$\frac{\mathrm{d}V}{\mathrm{d}t}=-\frac{3}{16}C_D Re_0\frac{V^2}{R\bar{\rho}_l},$$

where C_D is droplet drag coefficient.

The gas phase transport and thermodynamic properties are calculated as functions of temperature, pressure and composition. The liquid phase properties are calculated as functions of temperature and composition only. Zhang (2000) offered a detailed description on how the transport and thermodynamic properties for both phases and the interface mass fractions from vapor-liquid equilibrium were calculated. Real gas effects are modeled using the Peng–Robinson equation of state with appropriate binary interaction parameters and mixing rules, which are recommended by Reid et al. (1987).

3. Numerical method

The gas and liquid phase solutions were obtained using the axisymmetric unsteady equations of mass, species, momentum, and energy conservation in spherical coordinates. The equations are solved iteratively and coupled via the conservation equations at the interface. The finite-volume (Patankar, 1980) and SIMPLEC (Van Doormaal and Raithby, 1984) methods are used to discretize the governing equations in the computational domain. Uniform grid-spacing is used in the polar direction and liquid phase radial direction. An exponential stretching function is used to concentrate grid points near the droplet surface in the gas phase. Stagerred grids and hybrid scheme are used in the discretized equations. The general discretized equation can be expressed simply as

$$a_P\phi_P=\sum a_{nb}\phi_{nb}+b,$$

where a_P, a_{nb} are coefficients, b is source term, ϕ could be V_r, V_θ, T or Y_1, subscript nb indicates neighbor to grid point P and the summation is to be taken over all neighbors. The equations are solved by the *ADI* method. A TDMA solver is used along each of the two alternating directions and the numerical solution is obtained through iterations within a time step. The Euclidean norm of the residuals $\|r_\phi\|$ is used as the convergence criterion. The Euclidean norm is given by

$$\|r_\phi\| = \left[\sum\left(\sum a_{nb}\phi_{nb} + b - a_P\phi_P\right)^2\right]^{1/2},$$

where the outer summation is over all the interior control volumes. The iteration is continued until the following criterion is satisfied:

$$\|r_\phi\|^k \leqslant \gamma_\phi \|r_\phi\|^0,$$

where $\|r_\phi\|^k$ is the corresponding norm after kth iteration and $\|r_\phi\|^0$ is calculated at the beginning of iterations. The value of the residual factor γ_ϕ is taken as 0.15 for velocity components, temperature and mass fraction. For the pressure correction, it is taken as 0.2, which is recommended by Van Doormaal and Raithby (1984). To accelerate convergence, the TDMA solver was modified as suggested by Van Doormaal and Raithby and a overrelaxation parameter of 1.85 was employed. The detailed description on numerical methods can be found in the reference by Zhang (2000).

The initial conditions for the droplet include: an initial radius (R_0), a specified uniform temperature (T_0), a uniform pressure equal to the environment pressure, zero velocity, and a fuel mass fraction of one. Gas phase calculations start with a specified temperature (T_∞) and pressure (p_∞), zero velocity, and a nitrogen mass fraction of one throughout the computational domain. Computations were executed on a Cray J90 and Sun Workstation.

Calculations were terminated when $(R/R_0)^2 \leqslant 0.2$, or when the critical state for the binary system was reached.

4. Results and discussion

The Fig. 2 shows that the numerical mole fraction of nitrogen at the droplet surface varying with ambient pressure under thermodynamic equilibrium at the surface temperature of 352.59 K, compared with the experimental data of *n*-heptane-nitrogen systems from Knapp et al. (1982). The numerical prediction (solid and dash-dot lines) agrees very well with the experimental data (circle and stars) for both vapor and liquid phases as shown in Fig. 2, which indicates that the methods employed in the numerical model are good enough to calculate the mole fraction of nitrogen and *n*-heptane at the droplet surface under thermodynamic equilibrium for different ambient pressures.

The numerical model developed in this study is also validated using the *n*-heptane experimental data of Nomura et al. (1996), which were obtained under micro-gravity conditions. The droplets were initially at room temperature ($T_0 = 300$ K was used in the simulations). Fig. 3 presents the time histories of $(d^*/d_0^*)^2$ for different ambient temperatures (471 and 741 K) at the ambient pressure of 0.1 MPa. The axisymmetric numerical model developed for this study was used in the

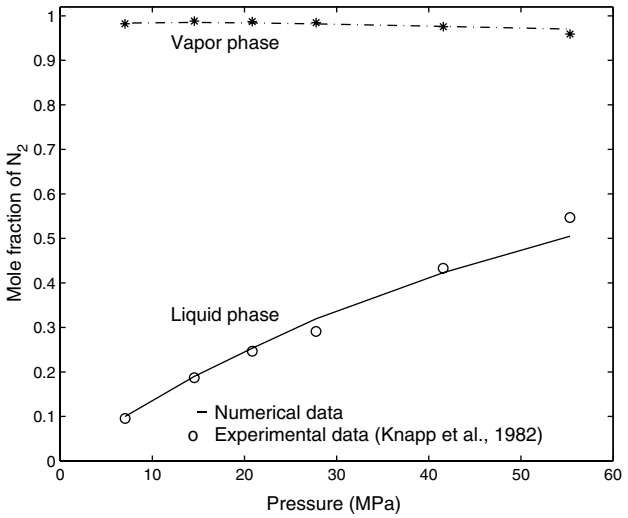

Fig. 2. The mole fraction of nitrogen at the droplet surface with ambient pressure for *n*-heptane-nitrogen systems at the surface temperature of 352.59 K.

limit case of very small initial droplet velocity ($V^*_{\infty,0} = 10^{-7}$ m/s) to simulate the experimental results of Nomura et al. (1996). These predictions (dashed lines) deviate from the measured data. The introduction of the droplet in the test position could be the main reason for this difference. The study by Nomura et al. (1996) aimed to provide data for stationary droplets evaporating

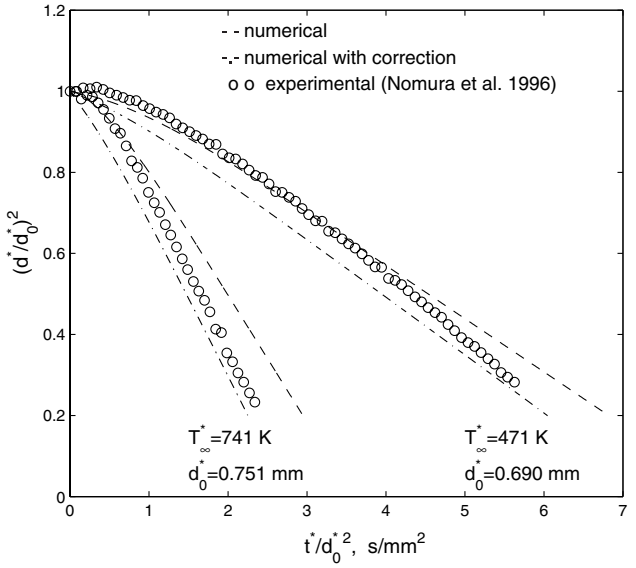

Fig. 3. Time histories of $(d^*/d_0^*)^2$ for different ambient temperature at the ambient pressure of 0.1 MPa (*note:* correction means initial droplet velocity is considered).

within a stagnant microgravity environment. However, as reported by Nomura et al. (1996) and Ristau et al. (1993), the droplet was moved from the droplet generator to the test position (a length of 60 mm) in 0.16 s within the hot nitrogen environment. This process introduced droplet motion at an average velocity of 0.375 m/s for 0.16 s. During this period the droplet experienced considerable heat-up. In addition, the shear stress at the liquid/gas interface introduced circulation within the droplet interior. The axisymmetric numerical model developed for this study can easily simulate the droplet motion and associated internal circulation as well as internal circulation that is sustained beyond the initial 0.16 s. When this effect is included the agreement between the experimental and the numerical results (dash-dot lines) is remarkable. The initial Reynolds number that was used for the case of the ambient temperature 471 K is 3.3, and is 4.4 for the ambient temperature 741 K. Similarly, for the ambient pressure of 1.0 MPa, the time histories of $(d^*/d_0^*)^2$ for different ambient temperatures (466 K with the initial Reynolds number of 74.0, and 765 K with the initial Reynolds number of 31.4) are plotted in Fig. 4. Nomura et al. (1996) presented nineteen cases such as these presented in Fig. 3 by varying ambient temperature and pressure. With a few exceptions, the excellent agreement as shown for these cases in Figs. 3 and 4 is obtained for the rest of the cases. The detailed comparison was obtained by Zhang (2000).

The following results are calculated for a moving *n*-heptane droplet evaporating into a nitrogen environment with an initial diameter of 100 μm and an initial temperature of 300 K for different ambient temperatures.

The dimensionless droplet diameter squared as a function of time for different ambient temperatures is plotted in Fig. 5 for the ambient pressure of 0.1 MPa, and in Fig. 6 for the ambient pressure of 4 MPa. Obviously, at the same ambient pressure, the droplet life time decreases with increasing ambient temperature due to faster evaporation at a higher ambient temperature. At the

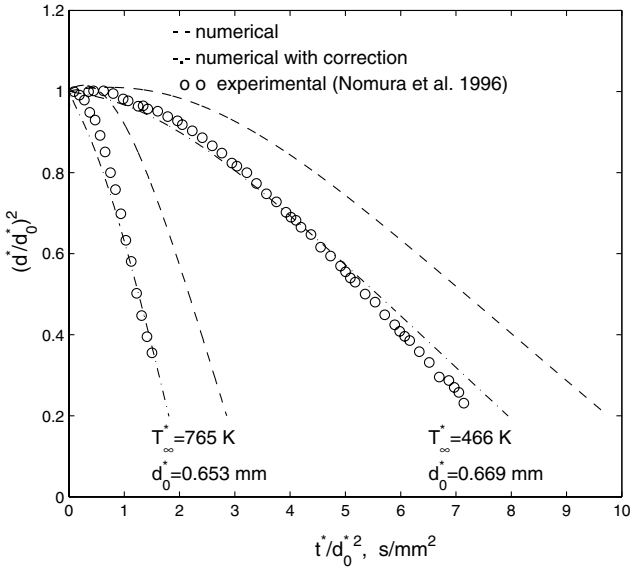

Fig. 4. Time histories of $(d^*/d_0^*)^2$ for different ambient temperature at the ambient pressure of 1.0 MPa (*note:* correction means initial droplet velocity is considered).

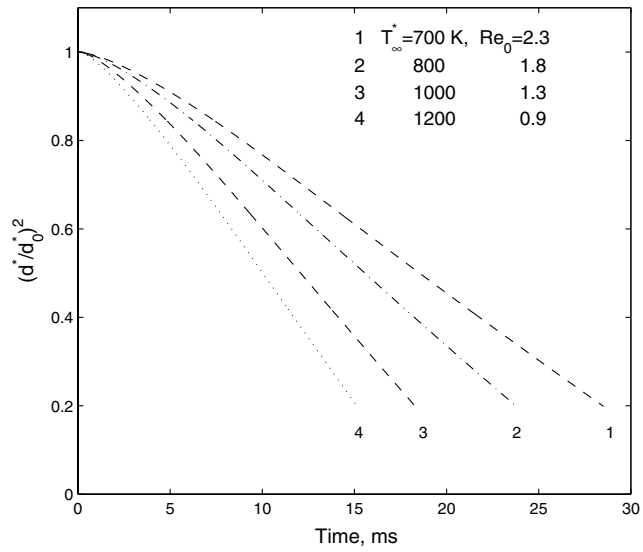

Fig. 5. Dimensionless diameter squared with time for different ambient temperatures ($p^*_\infty = 0.1$ MPa, $V^*_\infty = 1.5$ m/s).

low ambient pressure (0.1 MPa), the evaporation occurs immediately after the droplet is injected into the chamber, and the heat-up of the droplet is less important. However, at higher ambient pressure (4 MPa), droplet heat-up occurs for all ambient temperatures considered. The lower the ambient temperature, the longer the heat-up lasts. At higher ambient pressure the droplet swells initially due to the heat-up of the cold droplet and its subsequent regression rate is far from following the d^2-law during the early stages of droplet evaporation. However, the droplet presents

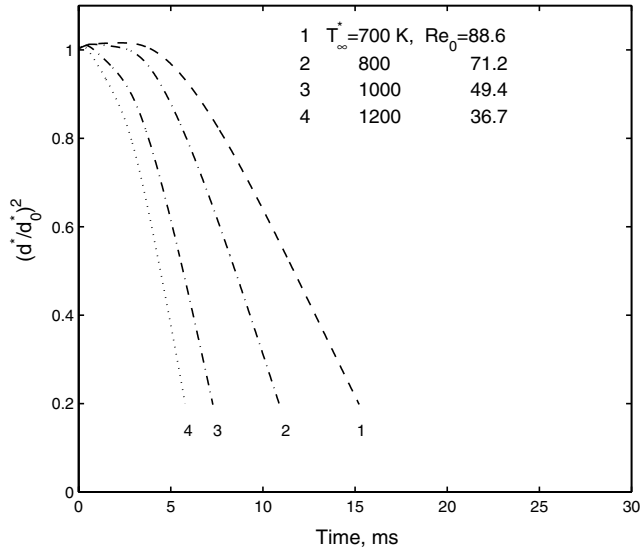

Fig. 6. Dimensionless diameter squared with time for different ambient temperatures ($p^*_\infty = 4.0$ MPa, $V^*_\infty = 1.5$ m/s).

an almost d^2-law behavior in later stages of droplet evaporation for all considered pressures (up to 4 MPa) in Figs. 5 and 6. These conclusions agree with the numerical results of Arias-Zugast et al. (2000).

Fig. 7 shows the average droplet evaporation constant as a function of ambient temperature for different ambient pressures. The droplet evaporation constant K is defined as $d_0^2 - d^2 = K(t - t_0)$, where d is the instantaneous droplet diameter, d_0 is the initial droplet diameter, t is time. Here, the droplet evaporation constant is defined as the average evaporation constant when the dimensionless droplet radius squared is less than 0.5 as employed by Ristau et al. (1993). Fig. 7 shows that the average evaporation constant increases with increasing ambient prdessure or increasing ambient temperature. At the lower ambient pressure of 0.1 MPa, the evaporation constant increases almost linearly with ambient temperature over the range of temperatures considered ($600 \leqslant T_\infty^* \leqslant 1200$). At higher ambient pressures, even though the average evaporation constant increases with the ambient temperature, however, the increasing rate of the average evaporation constant with the ambient temperature becomes smaller at high ambient temperature such as 1200 K.

Fig. 8 shows the droplet lifetime as a function of ambient temperature for different ambient pressures. Obviously, for the ambient temperatures and pressures considered, the droplet lifetime decreases with increasing ambient pressure or increasing ambient temperature.

Fig. 9 shows the final droplet penetration distance as a function of ambient temperature for different ambient pressures. The final penetration distance shown in Fig. 9 corresponds with the time that the calculations were terminated. Fig. 9 shows that the final penetration distance of the evaporating droplet decreases almost linearly with the ambient temperatures considered. Fig. 9 also shows that at the same ambient temperature, a higher ambient pressure results in a shorter final penetration distance.

Fig. 10 shows streamlines of droplet internal circulation for two different Reynolds numbers at the very early stage of droplet evaporation. The stream function ψ is defined by the dimensionless

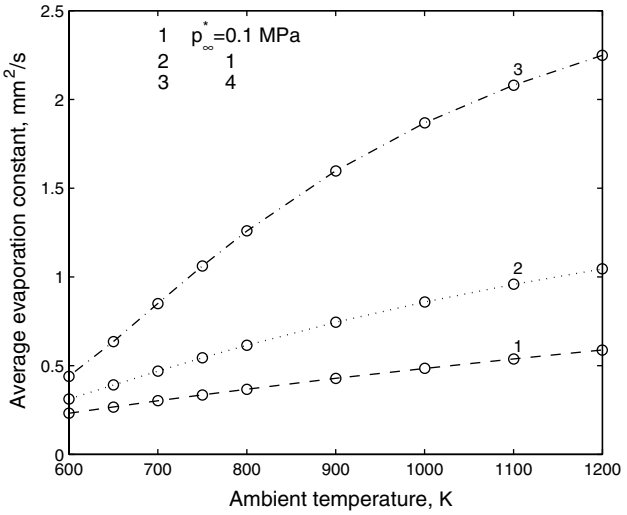

Fig. 7. Average evaporation constant with ambient temperature for different ambient pressures ($V_\infty^* = 1.5$ m/s).

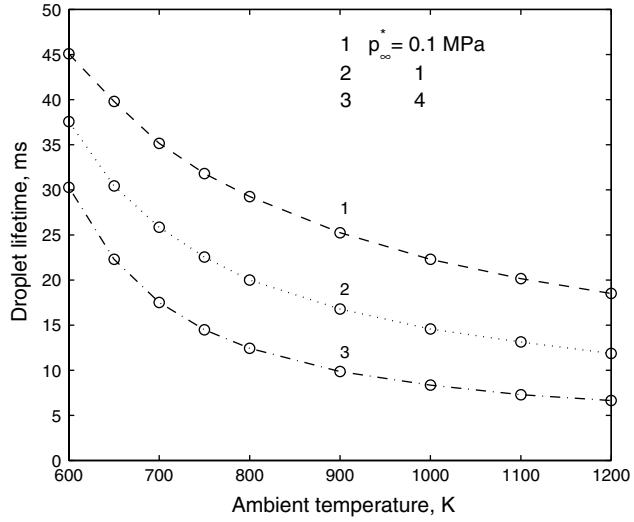

Fig. 8. The droplet lifetime with ambient temperature for different ambient pressures ($V^*_\infty = 1.5$ m/s).

variables: $V_r = -\frac{1}{\rho r^2 \sin\theta}\frac{\partial\psi}{\partial\theta}$ and $V_\theta = -\frac{1}{\rho r \sin\theta}\frac{\partial\psi}{\partial r}$. Fig. 10(a) has an initial Reynolds number of 71.2, and Fig. 10(b) has a larger initial Reynolds number, which is 213.6. Streamlines of internal circulation in Fig. 10(a) has the largest number as −0.1, however in Fig. 10(b) it is −0.125. Here the sign '−' means internal circulations instead of the external flow field. Larger Reynolds number (stronger external convection) causes stronger internal circulations, which causes quicker heat-up of liquid droplet. The more heat exchange between gas and liquid phases due to stronger internal circulation finally results in larger droplet regression rate as shown in case (b) in Fig. 11.

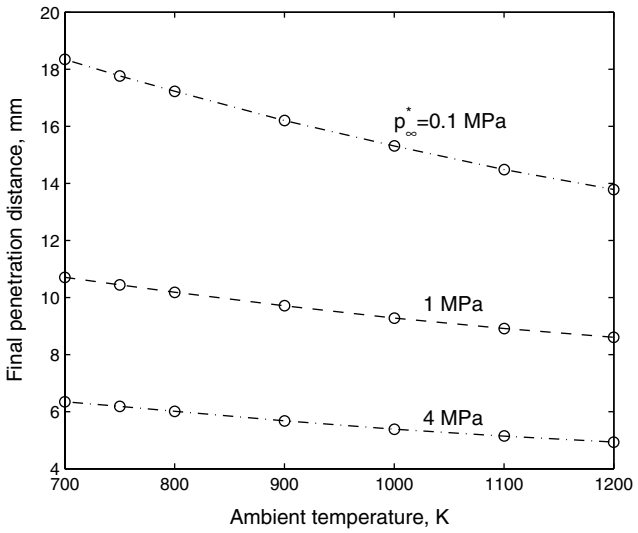

Fig. 9. The droplet final penetration distance at various ambient temperatures ($V^*_\infty = 1.5$ m/s).

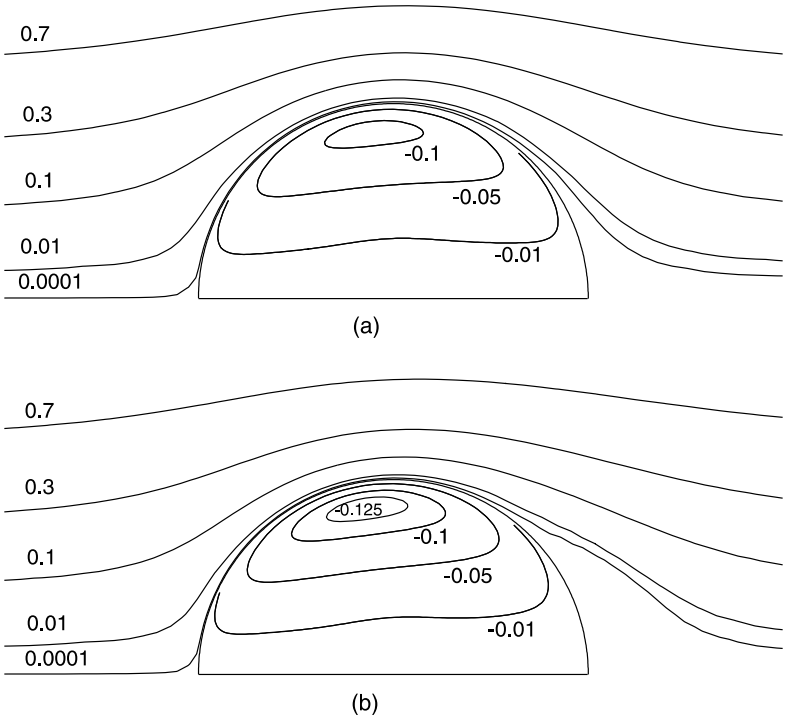

Fig. 10. The streamlines of internal circulation with different initial Reynolds numbers ($p^*_\infty = 4.0$ MPa, $T^*_\infty = 800$ K).

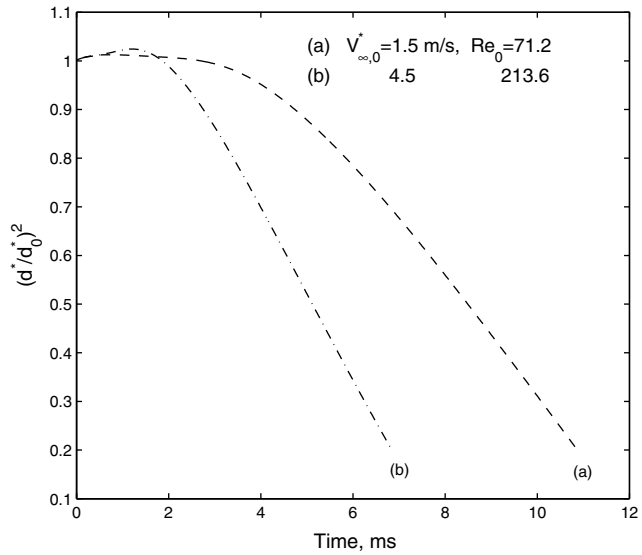

Fig. 11. Dimensionless diameter squared with time for different initial Reynolds numbers ($p^*_\infty = 4.0$ MPa, $T^*_\infty = 800$ K).

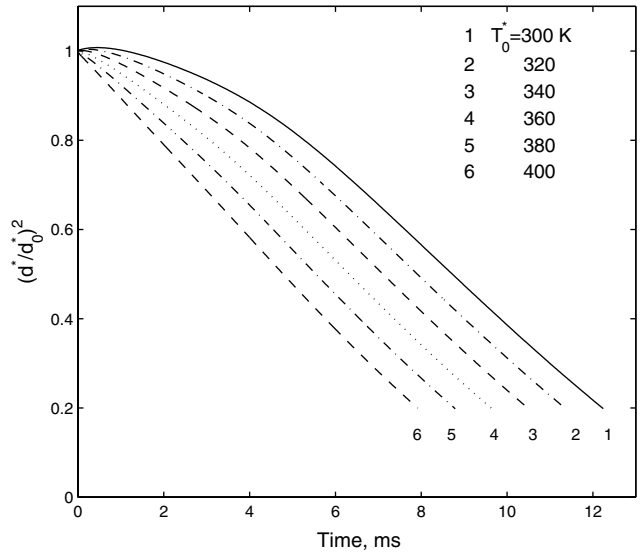

Fig. 12. Dimensionless diameter squared with time for different initial droplet temperatures ($p^*_\infty = 1.0$ MPa, $V^*_\infty = 1.5$ m/s).

The following results are calculated for a moving *n*-heptane droplet evaporating into a nitrogen environment (1000 K) with an initial diameter of 100 μm and different initial temperatures.

Fig. 12 shows the dimensionless droplet diameter squared as a function of time for different initial droplet temperatures at an ambient pressure of 1 MPa. Fig. 13 is the dimensionless droplet

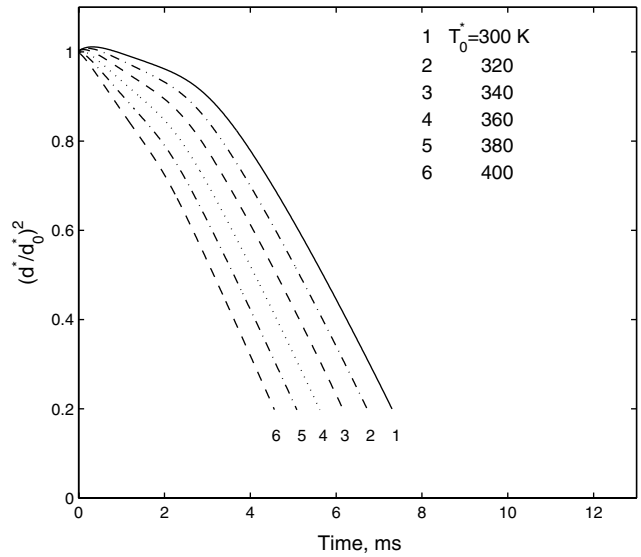

Fig. 13. Dimensionless diameter squared with time for different initial droplet temperatures ($p^*_\infty = 4.0$ MPa, $V^*_\infty = 1.5$ m/s).

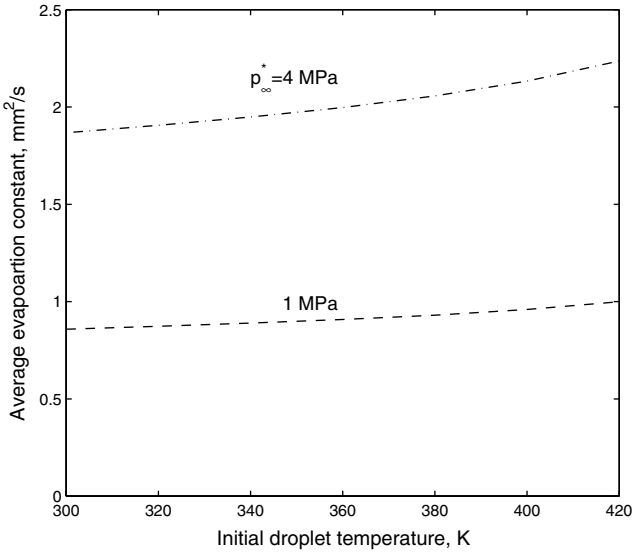

Fig. 14. Average evaporation constant with initial droplet temperature for different ambient pressures ($V_\infty^* = 1.5$ m/s).

diameter squared with time for different initial droplet temperatures at an ambient pressure of 4 MPa. At the same ambient temperature and pressure, the droplet lifetime decreases with increasing initial droplet temperature due to faster evaporation at a higher initial droplet temperature. At the low initial droplet temperature, the heat-up of the droplet is obvious. However, at higher initial droplet temperatures, the evaporation of the droplet occurs immediately after the droplet is injected into the chamber. At the same ambient pressure, curves in Figs. 12 or 13 are almost parallel at the later stages of the droplet evaporation, which means that all cases have the almost same average evaporation constant as shown in Fig. 14 since the isothermal conditions are almost achieved in the later stages of the droplet evaporation.

5. Conclusions

A comprehensive numerical model is developed to study a vaporizing fuel droplet (*n*-heptane) in a forced convective environment under different temperature conditions, which includes high pressure effects, real gas effects, liquid phase internal circulation, variable thermophysical properties, solubility of inert species into the liquid phase, and gas and liquid phase transients. The finite-volume (Patankar, 1980) and SIMPLEC (Van Doormaal and Raithby, 1984) methods are used to discretize the governing axisymmetric unsteady equations of mass, species, momentum, and energy conservation in the computational domain. An exponential stretching function is used to concentrate grid points near the droplet surface in the gas phase. Stagerred grids and hybrid scheme are used in the discretized equations.

Numerical predications of time histories of the dimensionless diameter square of a vaporizing fuel droplet within a zero gravity environment are in very good agreement with the microgravity experimental data of Nomura et al. (1996).

The numerical results show that at higher ambient pressure (such as 4 MPa) the droplet swells initially due to the heat-up of the cold droplet and its subsequent regression rate is far from following the d^2-law during the early stages of droplet evaporation. However, at the ambient pressure of 0.1 MPa, the effect of the heat-up counteracts the effect of the droplet evaporation, and the droplet swells are not obvious. The droplet presents an almost d^2-law behavior in later stages of droplet evaporation for all considered pressures (up to 4 MPa). At the lower ambient pressure of 0.1 MPa, the evaporation constant increases almost linearly with ambient temperature over the range of temperatures considered ($600 \leqslant T_\infty^* \leqslant 1200$). At higher ambient pressures, even though the average evaporation constant increases with the ambient temperature, however, the increasing rate of the average evaporation constant with the ambient temperature becomes smaller at high ambient temperature such as 1200 K. The numerical results also show that the droplet lifetime decreases with increasing ambient temperature. For example, the droplet lifetime at the ambient temperature 1200 K can be only 50–60% of the droplet lifetime at the ambient temperature 600 K. The final penetration distance of the vaporizing droplet decreases almost linearly with the ambient temperatures considered.

For the same ambient temperature and pressure, the droplet lifetime decreases with increasing initial droplet temperature due to faster evaporation at a higher initial droplet temperature. However, at the later stages of the droplet evaporation, the almost same average evaporation constant exists for different initial droplet temperatures.

Acknowledgements

The support from University of Nebraska-Lincoln, which provided the SGI O2000, Cray J90, and Sun Workstations for my studies, is greatly appreciated.

References

Arias-Zugast, M., Garcia-Ybarra, P.L., Castillo, J.L., 2000. Unsteady effects in droplet vaporization lifetime at subcritical and supercritical conditions. Combust. Sci. Technol. 153, 179–191.

Canada, G.S., Faeth, G.M., 1973. Fuel droplet burning rates at high pressures. Proceedings of the Combustion Institute 14, 1345–1354.

Chiang, C.H., Raju, M.S., Sirignano, W.A., 1992. Numerical analysis of convecting, vaporizing fuel droplet with variable properties. Int. J. Heat Mass Transfer 35, 1307–1324.

Curtis, E.W., Farrell, P.V., 1992. A numerical study of high-pressure droplet vaporization. Combust. Flame 90, 85–102.

Dandy, D.S., Leal, L.G., 1989. Buoyancy-driven motion of a deformable drop through a quiescent liquid at intermediate Reynolds numbers. J. Fluid Mech. 208, 161–192.

Delplanque, J.P., Sirignano, W.A., 1991. Transient vaporization and burning for an oxygen droplet at sub-and near-critical conditions. AIAA Paper 91-0075.

Delplanque, J.P., Sirignano, W.A., 1993. Numerical study of the transient vaporization of an oxygen droplet at sub- and super-critical conditions. Int. J. Heat Mass Transfer 36, 303–314.

Dwyer, H.A., 1989. Calculations of droplet dynamics in high temperature environments. Prog. Energy Combust. Sci. 15, 131–158.

Faeth, G.M., 1977. Current status of droplet and liquid combustion. Prog. Energy Combust. Sci. 3, 191–224.

Faeth, G.M., 1983. Evaporation and combustion of sprays. Prog. Energy Combust. Sci. 9, 1–76.

Givler, S.D., Abraham, J., 1996. Supercritical droplet vaporization and combustion studies. Prog. Energy Combust. Sci. 22, 1–28.

Haldenwang, P., Nicoli, C., Daou, J., 1996. High pressure vaporization of LOX droplet crossing the critical conditions. Int. J. Heat Mass Transfer 39, 3453–3464.

Haywood, R.J., Nafziger, R., Renksizbulut, 1989. A detailed examination of gas and liquid phase transient processes in convective droplet evaporation. J. Heat Transfer 111, 495–502.

Hsieh, K.C., Shuen, J.S., Yang, V., 1991. Droplet vaporization in high-pressure environment I: near critical conditions. Combust. Sci. Technol. 76, 111–132.

Kadota, T., Hiroyasu, H., 1976. Evaporation of a single droplet at elevated pressures and temperatures. Bull. JSME 19, 1515–1521.

Knapp, H., Doring, R., Oellrich, L. Plocker, U., Prausnitz, J.M., 1982. Vapor-Liquid Equilibria for Mixtures of Low Boiling Substances, Chemical Engineering Data Series, VI, Dechema, Frankfurt.

Law, C.K., 1982. Recent advances in droplet vaporization and combustion. Prog. Energy Combust. Sci. 8, 171–201.

Manrique, J.A., Borman, G.L., 1969. Calculations of steady state droplet vaporization at high ambient pressure. Int. J. Heat Mass Transfer 12, 1081–1095.

Matlosz, R.L., Leipziger, S., Torda, T.P., 1972. Investigation of liquid droplet evaporation in a high temperature and high pressure environment. Int. J. Heat Mass Transfer 15, 831–852.

Megaridis, C.M., Sirignano, W.A., 1990. Numerical modeling of a vaporizing multicomponent droplet. Proceedings of the Combustion Institute 23, 1413–1421.

Nomura, H., Ujiie, Y., Rath, H.J., Sato, J., Kono, M., 1996. Experimental study on high pressure droplet evaporation using microgravity conditions. Proceedings of the Combustion Institute 26, 1267–1273.

Patankar, S.V., 1980. Numerical Heat Transfer and Fluid Flow. Hemisphere Publishing Corporation, New York.

Poplow, F., 1994. Numerical calculation of the transition from subcritical droplet evaporation to supercritical diffusion. Int. J. Heat Mass Transfer 37, 485–492.

Prakash, S., Sirignano, W.A., 1980. Theory of convective droplet vaporization with unsteady heat transfer in the circulating liquid phase. Int. J. Heat Mass Transfer 23, 252–268.

Reid, R.C., Prausnitz, J.M., Poling, B.E., 1987. The Properties of Gases and Liquids, fourth ed. McGraw-Hill, Inc, New York.

Renksizbulut, M., Yuen, M.C., 1983. Numerical study of droplet evaporation in a high-temperature stream. J. Heat Transfer 105, 389–397.

Ristau, R., Nagel, U., Iglseder, H., Konig, J., Rath, H.J., Normura, H., Kono, M., Tanabe, M., Sato, J., 1993. Theoretical and experimental investigations on droplet evaporation and droplet ignition at high pressures. Microgravity Sci. Technol. VI/4, 223–228.

Rosner, D.E., Chang, W.S., 1973. Transient evaporation and combustion of a fuel droplet near its critical temperature. Combust. Sci. Technol. 7, 145–158.

Sato, J., Tsue, M., Niwa, M., Kono, M., 1990. Effects of natural convection on high-pressure droplet combustion. Combust. Flame 82, 142–150.

Sirignano, W.A., 1983. Fuel droplet vaporization and spray combustion theory. Prog. Energy Combust. Sci. 9, 291–322.

Van Doormaal, J.P., Raithby, G.D., 1984. Enhancements of the simple method for predicting incompressible fluid flows. Numer. Heat Transfer 7, 147–163.

Zhang, H., 2000. Evaporation of a spherical moving fuel droplet over a wide range of ambient pressures within a nitrogen environment. Ph.D. dissertation, University of Nebraska-Lincoln, Lincoln, Nebraska.

Zhang, H., Gogos, G., 2001. Droplet evaporation within a zero gravity high pressure and high temperature convective environment, in: Proc. of International Conference on Power Engineering, October 8–12, 2001, Xi'an, China, Vol. 2, pp. 1613–1620.